

Upper critical field of V-Ag multilayered superconductors

K. Kanoda, H. Mazaki, N. Hosoi, and T. Shinjo

Institute for Chemical Research, Kyoto University, Uji 611, Japan

(Received 15 September 1986)

We report investigations of the upper critical field ($H_{c2\perp}$ and $H_{c2\parallel}$) of V-Ag proximity-coupled superconducting multilayer structures, prepared by ultrahigh-vacuum electron-beam evaporation. By means of x-ray diffraction analysis, successful formation of an artificial superstructure is confirmed. From resistivity measurement parallel to the layers, the electron mean free paths in the V and Ag layers are determined. With reference to these transport properties, characterization of H_{c2} has been made. For three-dimensional multilayer structures, H_{c2} is analyzed in terms of the temperature dependence of $H_{c2\perp}$, the zero-temperature coherence length, and the anisotropy $H_{c2\parallel}/H_{c2\perp}$. Our results are in quantitative agreement with the relevant theories. For quasi-two-dimensional multilayer structures, a peculiar temperature dependence has been revealed in both $H_{c2\perp}$ and $H_{c2\parallel}$. $H_{c2\perp}$ exhibits positive curvature near T_c , and it is continuously enhanced with the increase of multilayer period, as predicted theoretically. In contrast with the monotonic variation in $H_{c2\perp}$, a drastic upturn at a certain temperature (dimensional crossover) and an upward inflection at a higher temperature have been observed in $H_{c2\parallel}$. These two types of anomalies in $H_{c2\parallel}$ are discussed in the context of the commensurability between the multilayer structure and the vortex lattice.

I. INTRODUCTION

Alternate deposition of superconducting and nonsuperconducting elements produces a new class of superconductors.¹ Generally speaking, such multilayered superconductors have two aspects; on one hand, they possess the nature of a single superconductor as a whole due to the long coherence length, and on the other hand they have the composite nature of the multilayered structure. With the variation of layer thickness, the competition between these two natures provides a rich variety of physical properties.²

The above situation is reflected most dramatically in the upper critical field H_{c2} as dimensional crossover, which was predicted by Klemm, Luther, and Beasley³ for Josephson-coupled multilayers. Indeed, Ruggiero, Barbee, Jr., and Beasley⁴ first demonstrated experimentally dimensional crossover in Nb-Ge Josephson-coupled multilayers. As for S (superconducting metal)-N (normal metal) multilayers, Banerjee *et al.*⁵ and Chun *et al.*⁶ found a similar crossover in the Nb-Cu system, and pointed out that the concept put forward in the theory of Josephson-coupled superconductors is also valid for the proximity-coupled system.

Since experimental study to date on dimensional crossover in S-N systems is limited to the specific system of Nb-Cu, it is worthwhile to investigate another combination of elements. In addition, to our knowledge there has been no systematic experiment on the variation of H_{c2} with S- and N-layer thicknesses in the three-dimensional regime.

In this work, we present a detailed study of H_{c2} of the V-Ag proximity-coupled superconducting multilayers, where we attempt to reveal an overall picture of characteristic behavior of H_{c2} as a function of layer thicknesses. Observed results are discussed in light of some existing theories. In what follows, we sketch the participating

theories on H_{c2} of S-N multilayers to make clear their relative characteristics.

The first theoretical study was by Dobrosavljević⁷ in the framework of the Ginzburg-Landau (GL) theory. Matching each solution of the respective GL equations in S and N layers through the boundary conditions, and assuming that an overall solution thus obtained, in turn, satisfies the anisotropic GL equation on macroscopic scale, he obtained the expressions for $H_{c2\perp}$ and $H_{c2\parallel}$, the upper critical field perpendicular and parallel to the layer.

Another approach was made by Ruggiero, Barbee, Jr., and Beasley⁴ (RBB), who developed the de Gennes-Werthamer theory,⁸ which gives the critical temperature in the absence of a magnetic field. They incorporated the pairbreaking effect of a magnetic field and then calculated the critical temperature in the presence of a field perpendicular to the layer near the zero-field transition temperature T_c . Thus they derived an analytical form for the temperature derivative of $H_{c2\perp}$ at T_c and its linear extrapolation to zero temperature $H_{c2\perp}(0)$.

The above two theories are practical for three-dimensional multilayers because of the simple analytical form of the results. However, the anomalous temperature dependence of H_{c2} observed in S-N multilayers is beyond them. We need, therefore, theories constructed at a more basic level, available in the full temperature region.

More recently, Biagi, Kogan, and Clem⁹ (BKC) calculated $H_{c2\perp}$ based on Eilenberger's theory and predicted a temperature dependence unseen in the conventional superconductors. A full curve of $H_{c2\perp}$ versus temperature is now obtainable, and calculations with appropriate parameters show that $H_{c2\perp}(T)$ gives a positive curvature near T_c . It is noted that the resultant BKC formula is essentially the same as RBB's.

Based on the de Gennes method, Takahashi and Tachiki¹⁰ (TT) calculated both $H_{c2\perp}$ and $H_{c2\parallel}$, where the

electron density of states, the diffusion constant of conduction electron, and the BCS electron-electron interaction constant are defined respectively in the S and N layers. Their exhaustive calculations show that the difference of these quantities in the S and N layers gives rise to rich variety of the temperature dependence of $H_{c2\perp}$ and $H_{c2\parallel}$. In particular, dimensional crossover in $H_{c2\parallel}$ is reproduced, and its systematic variation with layer thickness is given. This theory also shows that $H_{c2\perp}(T)$ has a positive curvature, which may be enhanced systematically by these parameters.

These theories are for dirty systems. As discussed later, the present V-Ag multilayers turn out to be dirty, so that application of the theories to our systems is justified.

This paper is organized as follows: In Sec. II, the sample preparation and structural characterization with x-ray analysis is presented. Transport properties, being necessary for discussion of H_{c2} , are also included in this section. The measurements, as well as some typical transition curves, are described in Sec. III. Our samples can be divided into two categories, i.e., one (with thinner layers) has three-dimensional character at all experimental temperatures, and the other (with thicker layers) shows quasi-two-dimensional behavior (occurrence of dimensional crossover). We present them separately in Secs. IV and V. In the former section, we first give a detailed analysis of the temperature dependence of $H_{c2\perp}$, and then discuss the coherence length and anisotropy of H_{c2} in terms of S- and/or N-layer thicknesses. In the latter section, we present dimensional crossover and anomalous inflection appeared in $H_{c2\parallel}$, and give a discussion in the context of the commensurability between the multilayer structure and the vortex lattice. We also study there the enhanced positive curvature observed in $H_{c2\perp}$. In Sec. VI conclusions are given.

Part of the results presented in this paper were reported briefly in our previous paper.¹¹

II. SAMPLE PREPARATION AND CHARACTERIZATION

A. Sample preparation

As the multilayered system, we chose a specific combination of V and Ag. The main reason for this selection is that they are not miscible in solid and even in liquid states, and hence alloy formation at the V-Ag interfaces is not expected.

The multilayered films were prepared by an ultrahigh-vacuum deposition method. The chamber was evacuated to about 10^{-10} Torr by a cryopump and kept in the 10^{-9} -Torr range during deposition. Two electron-beam guns (*e* guns) were used as vapor sources. As the evaporation sources V metal flakes of 99.9% purity were directly put in a water-cooled crucible of an *e* gun, and an Ag metal ingot of 99.9% purity was put on a Ta dish which was set in a crucible of another *e* gun to reduce heat dissipation. A liquid-N₂ trap was located around the heating devices in order to diminish outgassing. These materials were alternately deposited onto a mylar and/or a polyimide sheet and glass substrates at a rate of 0.3 Å/s.

TABLE I. Nominal structure, superconducting transition temperature, and resistivity of multilayered films. T_c is from the resistive transition. The samples with V layers thinner than 30 Å are mainly for structural study.

d_V/d_{Ag} (Å/Å)	Number of bilayers	T_c (K)	ρ ($\mu\Omega$ cm)
10/100	55		
15/30	30		
20/20	50		
20/40	50		
30/15	40	2.44	31.7
40/20	30	2.89	26.5
100/50	20	3.71	14.2
100/100	15	3.45	8.37
100/200	15	2.66	4.15
150/50	10	4.21	
160/320	10	2.88	3.01
200/400	10	3.48	2.36
240/480	7	3.40	2.03

We adopted a programmable quartz thickness monitor, of which the sensor head was placed near the substrate. To evaluate film thickness, only a geometrical factor was taken into account and other parameters were assumed to be the same as the bulk values. The thickness monitor actuates two shutters situated just above the evaporation sources at preset conditions to control film thickness. Two other sensor heads near the *e* guns monitor each evaporation rate of the sources irrespective of shutter motion. The substrate was kept at room temperature. No cooling was needed because the temperature increase during deposition was negligible. The first and the last layers of each sample are Ag. But for multilayers with Ag-layer thickness less than 100 Å, covering Ag layers were made 100 Å thick. The nominal structures of multilayers thus prepared are listed in Table I.

B. Structural characterization with x-ray analysis

The structure of V-Ag multilayered films was examined using a conventional powder diffractometer with Cu-K α radiation, keeping the scattering vector perpendicular or parallel to the film plane. The films on glass substrate were used for a perpendicular scan and those on polyimide sheet were for a parallel scan to get enough x-ray transmission. Since a mylar sheet gives a peak around V(110) in a parallel scan, it is not suitable for x-ray measurements.

Small-angle x-ray diffraction measurements were carried out to confirm the formation of artificial periodicity along the direction of film growth with the scattering vector perpendicular to the film plane. Several Bragg peaks corresponding to the artificial period were observed for all samples having multilayer periods shorter than 300 Å and thus they were directly proved to have periodic structure. Typical x-ray diffraction patterns are shown in Fig. 1. Since many higher-order peaks are detected, we expect the modulation mode of the periodic structure be nearly a square wave. In the samples with a longer period no

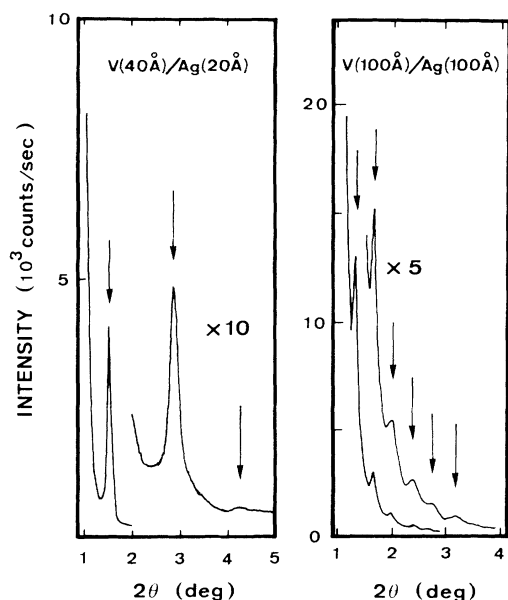


FIG. 1. Typical x-ray diffraction profiles for the multilayers in the small-angle region. Observed peaks are Bragg reflections corresponding to the artificial periodicity.

Bragg peak due to the artificial periodicity was observed, because the peak spacings were too close to be resolved. However, judging from the results for the samples with shorter period, we expect that the periodic structure is also established in those with a longer period.

The artificial period was determined from the observed Bragg peaks and compared with a sum of nominal thicknesses for single V and Ag layers. These results agree, proving that the film thickness measured by the thickness monitor is reliable. It was concluded from the small-angle x-ray diffraction that the designed superstructures were well established in the films.

The stacking structure of V and Ag layers was examined by scanning the higher-angle range. First we discuss the samples whose periods are shorter than 100 Å. Several peaks were observed around the calculated peak positions for bcc V(110) and fcc Ag(111), and no appreciable peaks were detected in the other region. This suggests that V(110) and Ag(111) planes are preferentially oriented parallel to the film plane. The x-ray diffraction patterns for some different compositions are presented in Fig. 2. They are not simple sum of V and Ag peaks, but consist of several ripples due to new reciprocal lattice points introduced by the artificial periodicity. Since the step model is known to be satisfactory for some metallic superstructures,¹²⁻¹⁴ reproduction of the observed patterns was attempted based on this simple model, where the following assumptions were made: First, the V(110) and Ag(111) planes are coherently stacked along the direction of film growth; second, the composition modulation is a square wave; third, the V and Ag layers maintain their bulk structures; and fourth, the interface plane spacing is an average of the V- and Ag-layer spacings. Calculated peak positions and intensities are shown in the lower part of

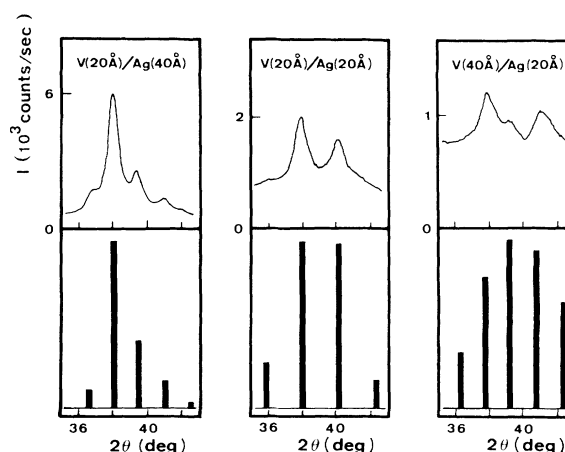


FIG. 2. Typical x-ray diffraction profiles for the multilayers with different compositions. Peak positions and intensities calculated on the basis of the step model are also shown in the lower figures.

Fig. 2. Despite its simplicity, the model simulates well the observed pattern of V (20 Å)-Ag (40 Å). It can be also applied to V (20 Å)-Ag (20 Å) (though the fitting becomes worse), but is not useful for V (40 Å)-Ag (20 Å). In order to simulate the pattern of the last sample, some parameters were adjusted in the framework of the model. The peak positions can be reproduced, but no reasonable agreement is achieved in the intensities.

From Fig. 2, we find that the peak width is broader and x-ray reflectivity is lower as the film composition becomes V rich. A similar tendency is seen when we compare V (15 Å)-Ag (30 Å) and V (30 Å)-Ag (15 Å). This suggests that the V-layer crystallinity of the superstructure changes systematically with the film composition. From the resistivity measurements, the crystal imperfection introduced in V is found to be much greater than that in Ag (see Sec. II C). This may be responsible for the above-mentioned result.

In the above discussion, the V and Ag layers were assumed to have their bulk structures. However, according to Brodsky,¹⁵ a thin Cr layer sandwiched by thick Au layers (fcc) changes its structure from bcc to fcc. To examine such a possibility in the V-Ag combination, x-ray diffraction measurements were carried out keeping the scattering vector parallel to the film plane, where the artificial periodicity gives no effect to the diffraction profiles. Observed peaks can be assigned assuming that V is bcc and Ag is fcc, and no evidence of fcc V appeared.

Samples with longer periods showed all peaks seen in the powder case in the perpendicular scan, but their intensities were different. This indicates that the preferential orientation of V(110) and Ag(111) planes which is seen in the samples with shorter periods still remains, but the degree of preferred orientation is not very high.

C. Transport properties

Any discussion of H_{c2} requires that we know the electron transport properties of the multilayer. For this pur-

pose, we measured the resistivity parallel to the layers ρ , where the films deposited on mylar sheets were cut into a strip ($1 \times 10 \text{ mm}^2$) and directly immersed in a liquid-He bath. Measurements were made with the four-probe method, where silver paint was used for the electric contact.

ρ just above T_c is shown in Fig. 3 as a function of Ag-layer thickness d_{Ag} .¹⁶ Numerical values of ρ are given in Table I. As seen in the figure, ρ decreases with increasing d_{Ag} . Referring to the change in ρ of the samples with the same thickness ratio $d_{\text{V}}:d_{\text{Ag}}$, we find that scattering at the V-Ag interface restricts substantially the mean free path of electrons in multilayers. However, if the boundary scattering is the only contribution to the resistivity, the slope of ρ versus d_{Ag} (or d_{V}) should be -1 . Deviation of the experimental points from the slope of -1 for a small period suggests that at least one of the intrinsic mean free paths within V and Ag layers is comparable to or smaller than the layer thickness.

In order to determine a practical value of mean free path l_{V} and l_{Ag} in the multilayers, we assume that ρ is given as a parallel junction of ρ_{V} and ρ_{Ag} (resistivities of V and Ag layers, respectively). Thus ρ is expressed as

$$\frac{1}{\rho} = \frac{d_{\text{V}}}{d_{\text{V}} + d_{\text{Ag}}} \frac{1}{\rho_{\text{V}}} + \frac{d_{\text{Ag}}}{d_{\text{V}} + d_{\text{Ag}}} \frac{1}{\rho_{\text{Ag}}} \quad (1)$$

As the first step, we attempted to evaluate ρ_{V} in the thick limit with otherwise prepared single V films. Observed resistivities scatter considerably ($20\text{--}35 \mu\Omega \text{ cm}$), probably due to surface oxidation. However, it is not unreasonable to suppose that ρ_{V} is $20 \mu\Omega \text{ cm}$ at most, which corresponds to $l_{\text{V}} \approx 20 \text{ \AA}$.¹⁷ On this supposition, we may say that for four samples denoted by solid circles in Fig. 3 ($d_{\text{V}} \geq 100 \text{ \AA}$), the contribution of boundary scattering in the V layers is so small that ρ_{V} in Eq. (1) be-

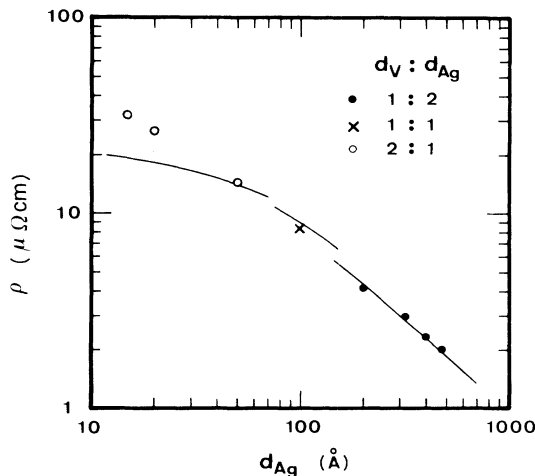


FIG. 3. Normal-state resistivity as a function of the Ag-layer thickness. Solid curves are calculated on the assumption of the bulk resistivity in the V layers ($15 \mu\Omega \text{ cm}$) and the thickness-dependent resistivity in the Ag layers.

comes constant, and hence the variation in ρ with the slope of nearly -1 is surely attributed to the boundary scattering of electrons in the Ag layers.

As is well known, Ag can be approximated as a free-electron system. In accordance with the Drude model, ρ_{Ag} is related to the mean free path l_{Ag} in the Ag layers by $\rho_{\text{Ag}} = 840/l_{\text{Ag}}$,¹⁸ where ρ_{Ag} is in unit of $\mu\Omega \text{ cm}$ and l_{Ag} is in \AA . Assuming the proportionality of l_{Ag} to the thickness d_{Ag} , we put $l_{\text{Ag}} = \alpha d_{\text{Ag}}$, where α is a constant. Thus we obtain $\rho_{\text{Ag}} = 840/\alpha d_{\text{Ag}}$. Since the second term in Eq. (1) is dominant for the above four samples, we can determine α by fitting the second term to the experimental results (solid circles) in Fig. 3, from which we get $\alpha = 1.3$, i.e., $l_{\text{Ag}} = 1.3d_{\text{Ag}}$. This relation is of course assumed applicable for all other experimental points in Fig. 3.

Once ρ_{Ag} is thus determined, substituting this value and the experimental values of ρ into Eq. (1), we can calculate ρ_{V} for other samples with smaller d_{Ag} , where the first term is comparable to the second term. Referring to the theoretical results of l_{V} versus ρ_{V} ,¹⁷ we find l_{V} versus d_{V} (see Fig. 4), where l_{V} decreases with decreasing d_{V} , reflecting the effect of V-Ag boundary scattering of electrons in thin V layers. At the same time, for V (100 \AA)-Ag (50 \AA) we get $\rho_{\text{V}} = 15 \mu\Omega \text{ cm}$, which corresponds to $l_{\text{V}} \approx 22 \text{ \AA}$. One can say that this value is almost the bulk value of this V, because l_{V} is several times smaller than d_{V} ($= 100 \text{ \AA}$).

To see how the effect of boundary scattering in the V layers appears in ρ ; we in turn substitute the bulk value $\rho_{\text{V}} = 15 \mu\Omega \text{ cm}$ into Eq. (1). Values of ρ thus calculated are given by solid curves in Fig. 3. Deviations of the two far left experimental points from the curve unambiguously indicate that in this region l_{V} is affected by the V-layer thickness.

Finally, we note that V and Ag layers are dirty in a superconductivity sense. The dirty nature of the V layers is evident from the short mean free path ($l_{\text{V}} \lesssim 22 \text{ \AA}$). As for the Ag layers, the coherence length ξ_{Ag} must be compared with the mean free path l_{Ag} , where $\xi_{\text{Ag}}(T) = (\hbar v_{\text{Ag}} l_{\text{Ag}} / 6\pi k_B T)^{1/2}$, and v_{Ag} is the Fermi velocity in Ag.¹⁹ Adopting the relation $l_{\text{Ag}} = 1.3d_{\text{Ag}}$, we estimate $\xi_{\text{Ag}}(T)$, of which the values at T_c as well as l_{Ag} are tabulated in Table II. Evidently $\xi_{\text{Ag}}(T_c) > l_{\text{Ag}}$ for all samples,

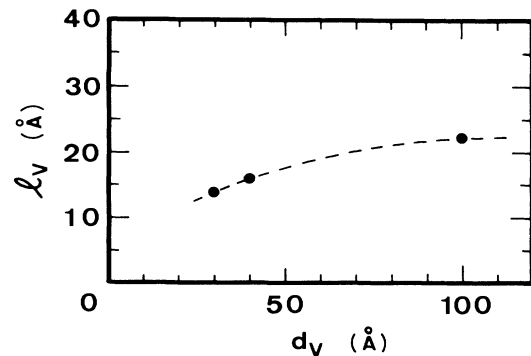


FIG. 4. Electron mean free path in the V layers as a function of the layer thickness.

TABLE II. Electron mean free paths and coherence lengths in the Ag layers.

d_V/d_{Ag} ($\text{\AA}/\text{\AA}$)	l_{Ag} (\AA)	$\xi_{Ag}(T_c)$ (\AA)
30/15	20	215
40/20	26	225
100/50	65	314
100/100	130	461
100/200	260	742
160/320	416	903
200/400	520	918
240/480	624	1020

although $\xi_{Ag}(T_c)$ approaches l_{Ag} in thicker Ag layers. Since $\xi_{Ag}(T)$ increases with decreasing temperature, the above inequality holds down to 0 K. Therefore we conclude that the Ag layers may also be treated in the dirty limit.

III. MEASUREMENTS

Prior to taking measurements of the upper critical field H_{c2} , the zero-field superconducting transition was observed by means of the ac and dc resistances, and also by the inductive change. Since all samples gave T_c below 4.2 K, measurements were made by soaking them in liquid He. Temperature was measured with a calibrated carbon glass resistor.

Each sample gave the same result in ac- and dc-resistance measurements. The inductive transition was observed by the use of a Hartshorn-type mutual inductance bridge, where the ac magnetic field (1.6–500 mOe) was applied perpendicular to the film plane cut into a 7-mm ϕ disk.

We show typical results in Fig. 5. The resistive transition width ΔT (10–90 % of normal resistance) is 20 mK. The real part χ' (in-phase component) of the inductive change shows a sharp transition to a complete diamagnetic state, and the imaginary part χ'' (out-of-phase component) forms a sharp, single peak in the transition region. Our previous work has revealed that superconductive inhomogeneity, if any, is well reflected in χ' and χ'' .²⁰ Although the inductive method alone is not sufficient to prove the existence of a bulk homogeneous transition,²¹ the observed shapes of χ' and χ'' , as well as their good coincidence with the resistive transition, firmly suggest a homogeneous transition over the sample. This has been also confirmed in a study of the penetration depth.²

We notice that samples with $d_{Ag} > 200 \text{\AA}$ exhibit a broad resistive transition width ($\Delta T > 0.1 \text{ K}$), while their inductive transition stays sharp. At this moment, we have no idea as to its origin.

The upper critical field $H_{c2\perp}$ and $H_{c2\parallel}$ were measured with the four-probe ac-resistance method down to 1.5 K. The current density ranges from 0.15 to 0.4 A/cm². At a fixed temperature, the magnetic field was swept up and down, where hysteresis was negligible and the transition width was 0.1 kG at best. In Fig. 6, we present the transition curves for the same sample in Fig. 5. H_{c2} was

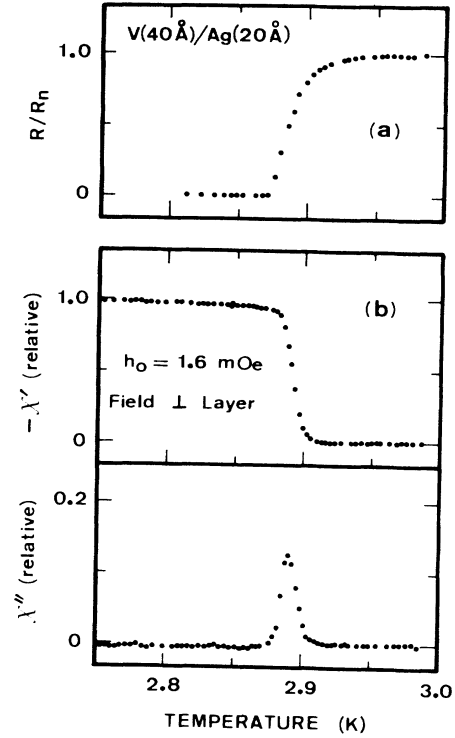


FIG. 5. (a) Resistive and (b) inductive transitions for V (40 \AA)-Ag (20 \AA) at zero magnetic field. χ' and χ'' are in-phase and out-of-phase components, respectively.

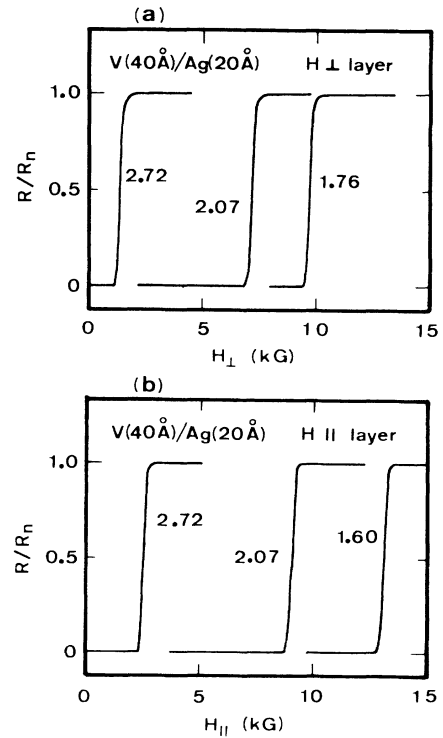


FIG. 6. Typical curves of the resistance vs magnetic field (a) perpendicular and (b) parallel to the layers. Numerical values in the figure are experimental temperatures.

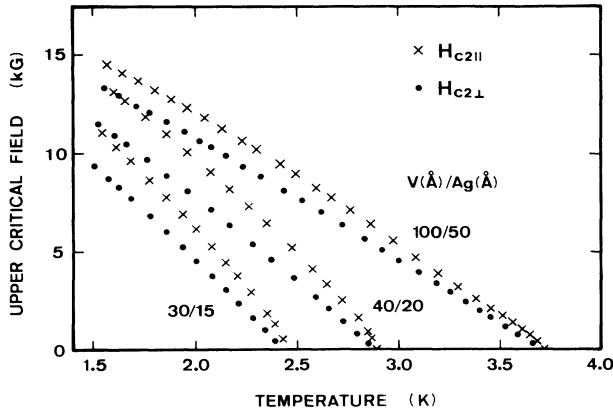


FIG. 7. Upper critical field for the multilayers with the same thickness ratio ($d_V:d_{Ag}=2:1$).

determined as the midpoint of the transition to the normal state. For a few samples with longer multilayer period, the transition curve with the field perpendicular to layer was broad, but the parallel case remained sharp.¹¹

In the measurement of H_{c2} , it is often necessary to consider surface superconductivity. We believe that this effect is substantially suppressed for the following reasons: First, both sides of each sample end with the Ag layers;²² second, in a proximity sandwich, when the conductivity of the normal metal is larger than that of the superconducting metal, the surface superconductivity tends to be suppressed.²³ This is the case in the present samples, in particular for those with longer multilayer period (see Sec. II C).

IV. THREE-DIMENSIONAL MULTILAYERS

This section is devoted to the results and discussion for multilayers (with thinner layers) which exhibit three-dimensional characteristics throughout the temperature available.

In Fig. 7 we show H_{c2} for multilayers with a constant thickness ratio ($d_V:d_{Ag}=2:1$), while in Fig. 8 we give H_{c2} for a constant d_V ($=100$ Å). Both H_{c21} and $H_{c2||}$ show a similar variation on the whole with temperature. The slight negative curvature of $H_{c2||}$ near T_c found for V (30 Å)-Ag (15 Å) and V (40 Å)-Ag (20 Å) is probably due to the effect of finite total thickness (~ 2000 Å), and is not

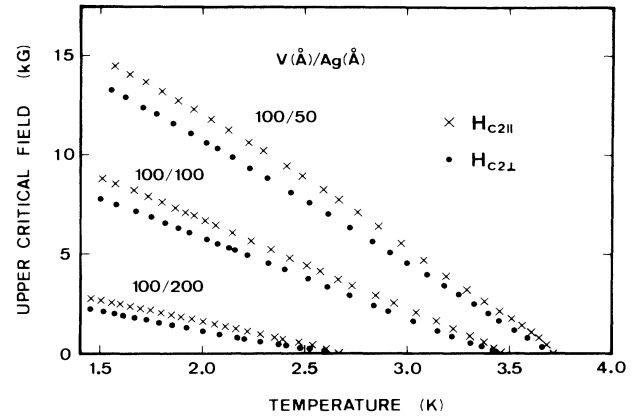


FIG. 8. Upper critical field for multilayers with the same V-layer thickness ($d_V=100$ Å).

essential from a viewpoint of multilayering.

We first discuss the temperature dependence of H_{c21} , and then examine the behavior of $H_{c21}(0)$ in terms of the zero-temperature coherence length parallel to the layer $\xi_{||}(0)$. Finally, we discuss the anisotropy $H_{c2||}/H_{c21}$. Characterization from these three aspects yields an overall picture of H_{c2} in three-dimensional multilayers. Calculated parameters in this section are listed in Table III.

A. Temperature dependence of H_{c21}

To examine the temperature dependence of H_{c21} , it is convenient to use the reduced upper critical field and temperature defined by

$$h_{c21}(t) = H_{c21}(t) / (-dH_{c21}/dt)_{t=1}, \quad t = T/T_c. \quad (2)$$

As seen in Fig. 8, H_{c21} exhibits a slight positive curvature immediately below T_c and then varies linearly with T . As the value of the slope is $-(dH_{c21}/dt)_{t=1}$, we adopt the linear portion. In this case, the reduced temperature t^* is defined using the transition temperature T_c^* extrapolated from the linear slope of $H_{c21}(T)$.

In Fig. 9 we show h_{c21} versus t^* for several samples. The result for V (40 Å)-Ag (20 Å) agrees well with the

TABLE III. Upper critical-field parameters for the three-dimensional multilayers.

d_V/d_{Ag} (Å/Å)	T_c^* (K)	$(dH_{c21}/dT)_{T_c^*}$ (kG/K)	$H_{c2 }/H_{c21}$	$\xi_{ }(0)$ (Å)	$\xi_{\perp}(0)$ (Å)
30/15	2.42	10.7	1.22	113	92.4
40/20	2.87	9.12	1.22	112	91.9
100/50	3.69	6.49	1.14	117	103
100/100	3.41	4.15	1.16	153	132
100/200	2.57	1.99	1.28	254	199

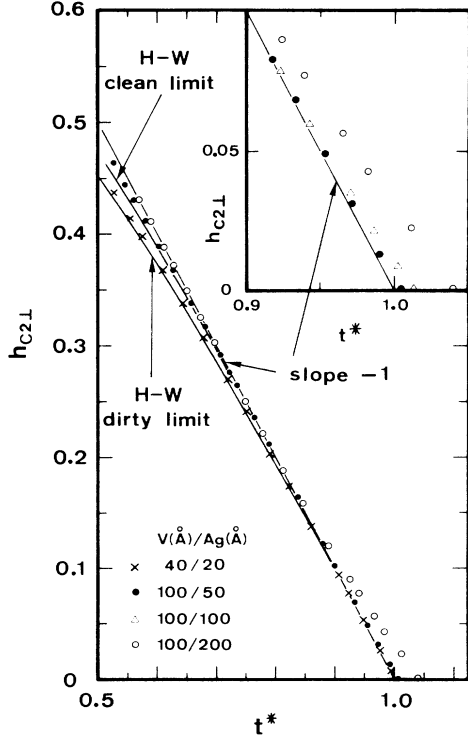


FIG. 9. Upper critical field perpendicular to the film plane vs temperature in reduced units. Inset expands the variation near $t^*=1$.

Helfand-Werthamer (HW) dirty-limit curve²⁴ throughout the experimental temperature range. V (30 Å)-Ag (15 Å) (not shown in the figure) falls on the same curve. This means that in the thin-layer limit, $h_{c2\perp}$ behaves like a conventional dirty-limit superconductor. For V (100 Å)-Ag (50 Å), however, $h_{c2\perp}$ shifts above the dirty-limit curve and even above the HW clean-limit curve.²⁴ The variation of $h_{c2\perp}$ becomes more peculiar for V (100 Å)-Ag (200 Å); near $t^*=1$; a positive curvature is appreciable, but $h_{c2\perp}$ shows a linear dependence at lower temperatures. Systematic appearance of the positive curvature is visible in the inset of Fig. 9.

Concerning a general tendency of $h_{c2\perp}$ described above, it is suggestive to comment on our results for the penetration depths of the same samples. In the thin-layer limit, the observed GL penetration depth is in good agreement with the value obtained from the Ginzburg-Landau-Abrikosov-Gor'kov relationship in the dirty limit,²⁵ while the results tend to deviate from it as the multilayer period becomes greater. Details will be published elsewhere.

B. Coherence length

The zero-temperature coherence length parallel to the layers is defined by

$$\xi_{\parallel}(0) = \left[-\frac{\phi_0}{2\pi(dH_{c2\perp}/dT)_{T_c^*} T_c^*} \right]^{1/2}, \quad (3)$$

where ϕ_0 is the flux quantum. As the slope of $H_{c2\perp}$ and the transition temperature, we adopt the linear portion of $H_{c2\perp}(T)$ and the extrapolated value T_c^* . In Fig. 10(a) is shown the variation of $\xi_{\parallel}(0)$ as a function of multilayer period d for the samples with the same compositional ratio ($d_V:d_{Ag}=2:1$). $\xi_{\parallel}(0)$ is shown to be insensitive to d . Figure 10(b) is for the samples where only d_{Ag} varies ($d_V=100\text{Å}$). In contrast to Fig. 10(a), $\xi_{\parallel}(0)$ increases considerably with d_{Ag} . We discuss these characteristics in terms of the RBB⁴ and BKC⁹ theories.

According to them, $H_{c2\perp}$ for S-N multilayers (the critical temperatures of the S and N layers are T_S and zero, respectively) is determined by solving the following equations:

$$q_S \tan(q_S d_S/2) = \eta q_N \tanh(q_N d_N/2), \quad (4)$$

$$q_S^2 = 2\pi k_B T y(t_S) / \hbar D_S - 2\pi H_{c2\perp} / \phi_0, \quad (5)$$

$$q_N^2 = 2\pi k_B T / \hbar D_N + 2\pi H_{c2\perp} / \phi_0, \quad (6)$$

$$\text{Int}_S = \psi(\frac{1}{2}) - \psi(\frac{1}{2} + y/2), \quad (7)$$

where $d_{S,N}$ are thicknesses of the S and N layers, $D_{S,N}$ are their diffusion constants, t_S is defined by T/T_S , $\psi(x)$ is the digamma function, and η denotes a parameter to characterize the boundary conditions at the S-N interface. The existence of the second term in the right-hand side of Eqs. (5) and (6) is the only point which distinguishes this

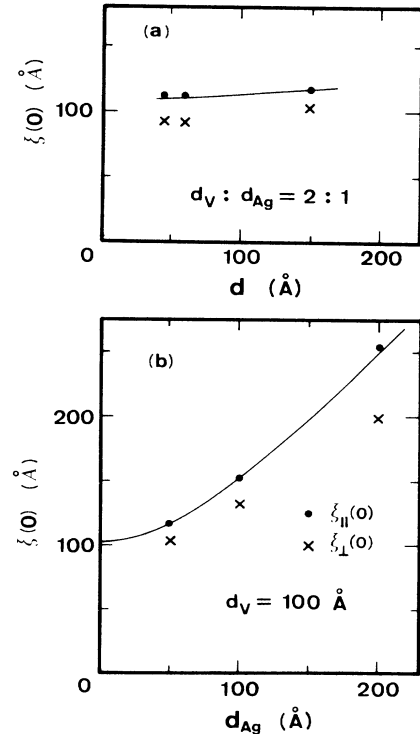


FIG. 10. The zero-temperature GL coherence length parallel and perpendicular to the layers for samples with (a) the same thickness ratio and (b) the same V-layer thickness. Solid curves show the calculated $\xi_{\parallel}(0)$ based on the RBB⁴ and BKC⁹ theories.

theory from the de Gennes-Werthamer theory for T_c .⁸ If $q_S d_S < 1$ and $q_N d_N < 1$, Eqs. (4)–(6) reduce to a single equation,

$$H_{c2\perp} = \frac{\phi_0 k_B T_y(t_S)}{\hbar D_S} \frac{1 - \eta [d_N D_S / d_S D_N \gamma(t_S)]}{1 + \eta (d_N / d_S)}. \quad (8)$$

Note that the factor $\phi_0 k_B T_y(t_S) / \hbar D_S$ represents H_{c2} of the S-layer material, because Eq. (7) combined with $H_{c2} = \phi_0 k_B T_y(t_S) / \hbar D_S$ leads to the Maki-de Gennes formula.²⁶ Thus we obtain

$$\xi_{\parallel}(0) = \xi_S(0) (1 + \eta d_N / d_S)^{1/2}, \quad (9)$$

where $\xi_S(0)$ is the zero-temperature GL coherence length in the S-layer material. Equation (9) implies that $H_{c2\perp}(0)$ for thin S-N multilayers never exceeds that of the S-layer material.

We apply this formula to our V-Ag multilayers. First, we determine η . Since it is given as a ratio of the conductivities of superconducting and normal layers in the dirty limit,²⁷ we can write

$$\eta = \frac{N_{Ag}(0) v_{Ag} l_{Ag}}{N_V(0) v_V l_V}, \quad (10)$$

where $N(0)$, v , and l are, respectively, the densities of state at the Fermi surface, the Fermi velocities, and the mean free paths in the V and Ag layers. In Eq. (10), we replace $N_{Ag}(0)/N_V(0)$ by γ_{Ag}/γ_V , the ratio of the electronic coefficients of specific heat. Numerical values used for γ and v are $\gamma_V = 1.15 \times 10^4$ erg/cm³K²,²⁸ $\gamma_{Ag} = 0.63 \times 10^3$ erg/cm³K²,²⁹ $v_V = 3.73 \times 10^7$ cm/s,¹⁷ and $v_{Ag} = 1.39 \times 10^8$ cm/s.²⁹ These values are for pure metals. It is well known that for the V metal, parameters involved in the band structure are affected by disorder.^{17,30} Therefore we must be careful in choosing γ_V and v_V , where the mean free path varies with layer thickness (see Fig. 4). Fortunately, according to Ref. 17, γ_V and v_V change inversely with the mean free path. This indicates that they tend to compensate each other by multiplication and hence the use of pure-metal values is acceptable. Thus, by substituting the numerical values into Eq. (10), Eq. (9) becomes

$$\xi_{\parallel}(0) = \xi_V(0) [1 + 0.204 (l_{Ag}/l_V) (d_{Ag}/d_V)]^{1/2}, \quad (11)$$

where $\xi_V(0)$ is the zero-temperature GL coherence length for the V layer. As already discussed in Sec. III C, $l_{Ag} = 1.3 d_{Ag}$ and l_V is given in Fig. 4.

A further step is to estimate $\xi_V(0)$ in Eq. (11). In the dirty limit, $\xi_V(0) \propto (\xi_{0V} l_V)^{1/2}$, where ξ_{0V} is the BCS coherence length for V. At first glance one might expect that $\xi_V(0)$ varies with l_V . According to Ref. 17, however, ξ_{0V} decreases with increasing l_V , and in particular for $l_V < 25 \text{ \AA}$, which is our case, $\xi_{0V} \propto 1/l_V$, suggesting that $\xi_V(0)$ is independent of the V-layer thickness of the multilayers in question. The constant parameter $\xi_V(0)$ was determined by substituting the experimental value $\xi_{\parallel}(0) = 117 \text{ \AA}$ for V (100 \AA)-Ag (50 \AA) into Eq. (11); $\xi_V(0) = 103 \text{ \AA}$.

Curves of $\xi_{\parallel}(0)$ thus calculated for the V-Ag multilayers are shown by solid curves in Fig. 10. Agreement of

the observed results with the calculated results is excellent.

In Fig. 10, we also show the coherence length perpendicular to the layer $\xi_{\perp}(0)$, which is defined by $\xi_{\perp}(0) = \xi_{\parallel}(0) (H_{c2\perp}/H_{c2\parallel})$, where the value of $H_{c2\perp}/H_{c2\parallel}$ is given below. The variation of $\xi_{\perp}(0)$ with d or d_{Ag} has a similar tendency to that of $\xi_{\parallel}(0)$.

It is interesting to compare $\xi_{\perp}(0)$ with that of Josephson-coupled multilayers, where $\xi_{\perp}(0)$ progressively decreases with the increase of insulating layer thickness.⁴ These two types of multilayers are in contrast with each other in view of the coherence length, although dimensional crossover is common to both.

C. Anisotropy of H_{c2}

We consider the anisotropic ratio $H_{c2\parallel}/H_{c2\perp}$ as a function of d or d_{Ag} . Since some samples exhibit a small curvature in H_{c2} immediately below T_c , we have to seek a linear portion for determination of the ratio. Since $H_{c2\parallel}/H_{c2\perp}$ is not sensitive to T except near T_c , we take the anisotropic ratio at $T/T_c = 0.6$, as shown in Fig. 11. On the whole, $H_{c2\parallel}/H_{c2\perp}$ is neither sensitive to d nor d_{Ag} . The ratio is found to weakly decrease with the increase of d [Fig. 11(a)] and to weakly increase with d_{Ag} [Fig. 11(b)].

According to Dobrosavljević,⁷ the anisotropy in H_{c2} for

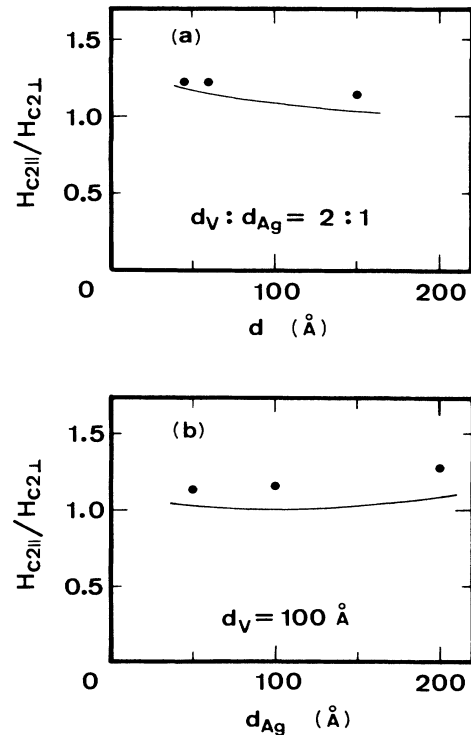


FIG. 11. Anisotropy of the upper critical field for samples with (a) the same thickness ratio and (b) the same V-layer thickness. Solid curves show the calculated anisotropy based on the Dobrosavljević theory.⁷

thin S-N multilayers is given by

$$\frac{H_{c2\parallel}}{H_{c2\perp}} = \frac{1}{1+d_N/d_S} [(1+\eta d_N/d_S)(1+d_N/\eta d_S)]^{1/2}, \quad (12)$$

where η is defined by Eq. (10). Equation (12) tells us that η plays an important role and $H_{c2\parallel}/H_{c2\perp} \geq 1$, where the minimum value ($H_{c2\parallel}/H_{c2\perp} = 1$) is taken at $\eta = 1$ irrespectively of d_S and d_N .

In Fig. 11 we also show the calculated curves given by Eq. (12), where η is evaluated in the same manner as in Sec. IV B. The relative dependence of $H_{c2\parallel}/H_{c2\perp}$ on d or d_{Ag} is reproduced well, but all the observed values lie slightly above the calculated curves. The surface superconductivity may be involved to some degree in causing this, even in the presence of covering Ag layers.

It is interesting to compare the present results with those of Josephson-coupled multilayers;⁴ the anisotropy in our case is much smaller than in the Josephson-coupled system, and is not sensitive to d_{Ag} , while in the Josephson-coupled multilayers, the anisotropy progressively increases with insulating layer thickness. This distinctive difference can be understood by recognizing that in the proximity-coupled multilayers the conductivity ratio η is a dominant factor for anisotropy, while in the Josephson-coupled system the tunneling which depends exponentially on insulating layer thickness is responsible.

The above feature involved in the proximity-coupled multilayers suggests that the system is more favorable for observing dimensional crossover in $H_{c2\parallel}$, because larger anisotropy in the Josephson-coupled system leads to a steeper slope of $H_{c2\parallel}$ in the three-dimensional temperature region, making the occurrence of the upturn indistinct.

V. QUASI-TWO-DIMENSIONAL MULTILAYERS

Investigation of the temperature dependence of $H_{c2\parallel}$ and $H_{c2\perp}$ for quasi-two-dimensional multilayers is the subject of this section. In Fig. 12, we show $H_{c2\parallel}$ and $H_{c2\perp}$ for four samples with the same thickness ratio of V and Ag (1:2), among which V (100 Å)-Ag (200 Å) having three-dimensional characteristics is included for reference. A systematic change is visible as the multilayer period d varies. In the following, discussion of these results is given.

A. $H_{c2\parallel}$

In Fig. 13, $H_{c2\parallel}$ is shown as a function of the reduced temperature t . Characteristic behavior emerges when d exceeds a certain limit. For V (100 Å)-Ag (200 Å), $H_{c2\parallel}$ varies linearly with t in a three-dimensional GL manner. For the samples with a longer period, however, there appear two types of anomalies in the curve of $H_{c2\parallel}(t)$.

First, for V (200 Å)-Ag (400 Å) and V (240 Å)-Ag (480 Å), a drastic upturn appears at the temperature t_A (denoted by A in the figure), and t_A shifts higher as d increases. This phenomenon is quite similar to the dimensional crossover observed in the Nb-Cu multilayers.⁶ Besides, TT calculations¹⁰ for $H_{c2\parallel}$ show that dimensional crossover in an S-N superlattice occurs above a certain threshold of d and its onset temperature becomes higher as d increases. Although quantitative comparison with the TT theory is not attainable at the present stage, qualitative

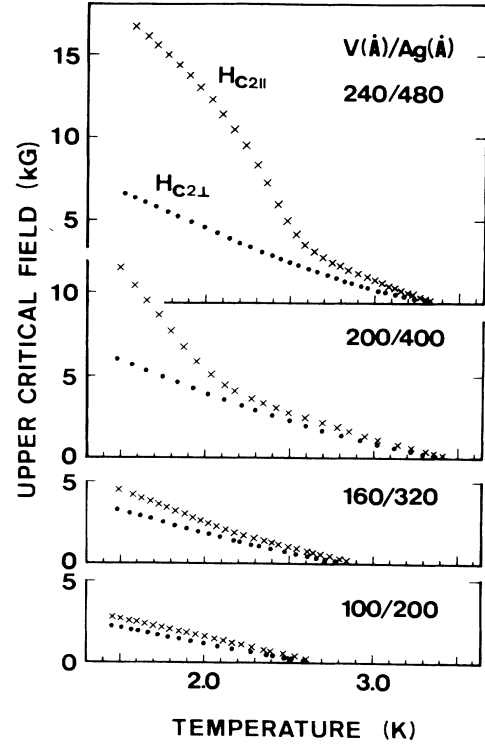


FIG. 12. Upper critical field for samples with longer multilayer period. The thickness ratio of V and Ag is 1:2.

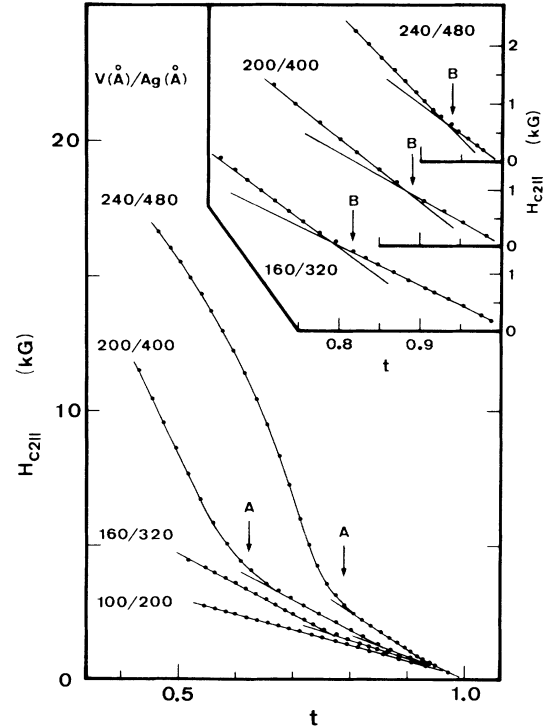


FIG. 13. Upper critical field parallel to the layer as a function of the reduced temperature. Thickness ratio of V and Ag is 1:2. Inset is an expanded figure, where upward inflections are visible. A and B indicate temperatures at which the upturn and the inflection start.

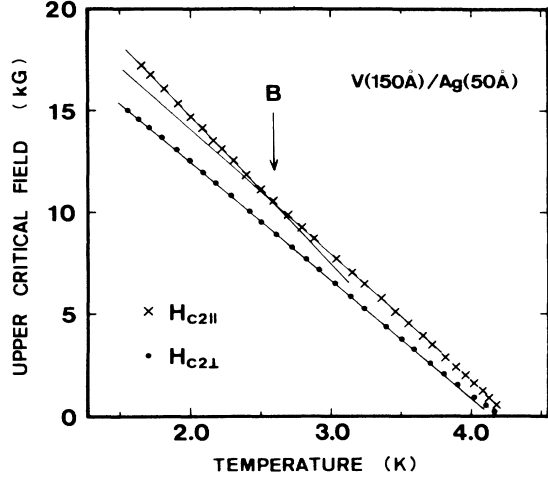


FIG. 14. Upper critical field as a function of temperature for V (150 Å)-Ag (50 Å). An upward inflection in the parallel upper critical field is visible at a temperature denoted by B . Solid lines serve as a guide for the eye.

features are in agreement. Further discussion is given below, shedding light on the coherence length.

As another anomaly, one finds an upward inflection at a higher temperature t_B in the curves of $H_{c2\parallel}(t)$ of V (160 Å)-Ag (320 Å), V (200 Å)-Ag(400 Å), and V (240 Å)-Ag (480 Å) (denoted by B in the inset of Fig. 13). Besides, the inflection temperature t_B systematically shifts higher with increasing d . This abrupt change in the curves of $H_{c2\parallel}(t)$ is not characteristic of the specific thickness ratio of V and Ag(1:2), but is also found for V (150 Å)-Ag (50 Å) (see Fig. 14). We emphasize that this anomaly in $H_{c2\parallel}$ is physically different from the gradual upturn in $H_{c2\perp}$ (see below).

To characterize the above two types of anomalies in $H_{c2\parallel}$, we start with an estimation of the coherence lengths at t_A and t_B . As the first approximation, we assume the anisotropic GL theory be valid down to t_A . In the theory, the upper critical field is related to the coherence lengths by³¹

$$H_{c2\perp}(t) = \frac{\phi_0}{2\pi\xi_{\parallel}^2(t)}, \quad (13)$$

$$H_{c2\parallel}(t) = \frac{\phi_0}{2\pi\xi_{\parallel}(t)\xi_{\perp}(t)}. \quad (14)$$

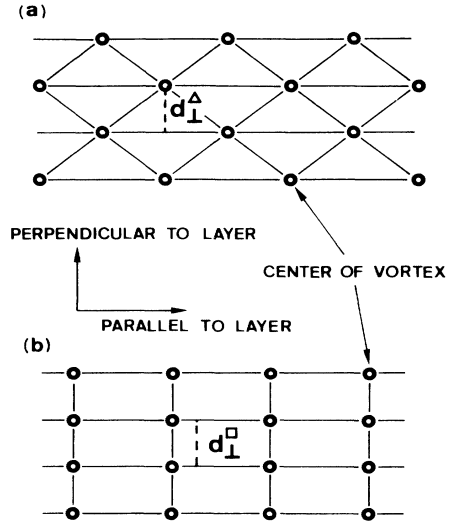


FIG. 15. (a) Triangular and (b) rectangular configurations of a vortex lattice. d_{\perp}^{Δ} and d_{\perp}^{\square} are the distance between vortex trains parallel to the layers.

Calculated values of ξ_{\parallel} and ξ_{\perp} at t_A and t_B are tabulated in Table IV. We find that $\xi_{\perp}(t_B)$ is exactly twice $\xi_{\perp}(t_A)$ for both V (200 Å)-Ag (400 Å) and V (240 Å)-Ag (480 Å). This fact strongly indicates that the upturns at t_A and t_B are closely correlated.

According to the work by Klemm, Luther, and Beasley,³ dimensional crossover takes place when $\xi_{\perp}(t)$ is of the order of insulating-layer thickness d_I in Josephson-coupled multilayers as far as superconducting-layer thickness d_S is negligible. For the case of finite d_S , Deucher and Entin-Wohlman³² showed that similar upturns occur when $\xi_{\perp}(t)$ becomes of the order, in turn, of the multilayer period $d (=d_S + d_I)$.

In accordance with their predictions, we focus our attention on the relation between d and ξ_{\perp} at t_A and t_B . However, our endeavor is to compare d with the lattice spacing of flux vortices which is given in terms of ξ_{\perp} , instead of a direct comparison of d and ξ_{\perp} .

Since the microscopic vortex structure in multilayered superconductors is not known, we examine two cases, triangular and rectangular lattices. We first assume that the vortices form a lattice deformed from an equilateral triangular with one side parallel to the layer, of which the deformation factors are $(\xi_{\parallel}/\xi_{\perp})^{1/2}$ parallel and $(\xi_{\perp}/\xi_{\parallel})^{1/2}$ perpendicular to the layer [see Fig. 15(a)]. These factors

TABLE IV. Calculated parameters at temperatures indicated by arrows A and B in Fig. 13, and second derivative of $H_{c2\perp}$ at T_c .

d_V/d_{Ag} (Å/Å)	A					B					$(d^2H_{c2\perp}/dT^2)_{T_c}$ (kG/K ²)
	t_A	ξ_{\perp} (Å)	ξ_{\parallel} (Å)	d_{\perp}^{Δ} (Å)	d_{\perp}^{\square} (Å)	t_B	ξ_{\perp} (Å)	ξ_{\parallel} (Å)	d_{\perp}^{Δ} (Å)	d_{\perp}^{\square} (Å)	
240/480	0.79	274	431	640	687	0.94	530	970	1237	1329	3.4
200/400	0.62	250	310	584	627	0.89	499	697	1163	1251	2.6
160/320						0.82	401	592	936	1005	1.7
100/200											0.72
150/50						0.61	163	191	380	409	

correspond to the deformation of vortex cores given by the anisotropic GL theory. At $H_{c2\parallel}$, the distance d_{\perp}^{Δ} between vortex trains parallel to the layer is expressed as³³

$$d_{\perp}^{\Delta} = (\frac{3}{4})^{1/4} (\phi_0 / H_{c2\parallel})^{1/2} (\xi_{\perp} / \xi_{\parallel})^{1/2}. \quad (15)$$

Substituting Eq. (14) into Eq. (15), we get

$$d_{\perp}^{\Delta} = 3^{1/4} \pi^{1/2} \xi_{\perp}. \quad (16)$$

Calculated values of d_{\perp}^{Δ} at t_A and t_B are tabulated in Table IV.

Next we consider the rectangular lattice where the square lattice is deformed in a similar manner to the case of triangular lattice [see Fig. 15(b)]. In this case, the distance d_{\perp}^{\square} between vortex trains at $H_{c2\parallel}$ becomes

$$d_{\perp}^{\square} = (\phi_0 / H_{c2\parallel})^{1/2} (\xi_{\perp} / \xi_{\parallel})^{1/2}. \quad (17)$$

Substitution of Eq. (14) into Eq. (17) yields

$$d_{\perp}^{\square} = (2\pi)^{1/2} \xi_{\perp}. \quad (18)$$

The calculated values of d_{\perp}^{\square} are also given in Table IV.

As listed in the table, the values of d_{\perp}^{Δ} and d_{\perp}^{\square} are so close that it is not essential which lattice is the case. However, one finds an important relation between d and d_{\perp}^{Δ} (d_{\perp}^{\square}); at t_A , d_{\perp}^{Δ} (d_{\perp}^{\square}) is almost equal to d , and at t_B , d_{\perp}^{Δ} (d_{\perp}^{\square}) is nearly twice d (see Fig. 16). This indicates that the observed upturns at t_A and t_B are the phenomena closely related to the commensurability between periodic superlattice structure and vortex lattice. That is, the vor-

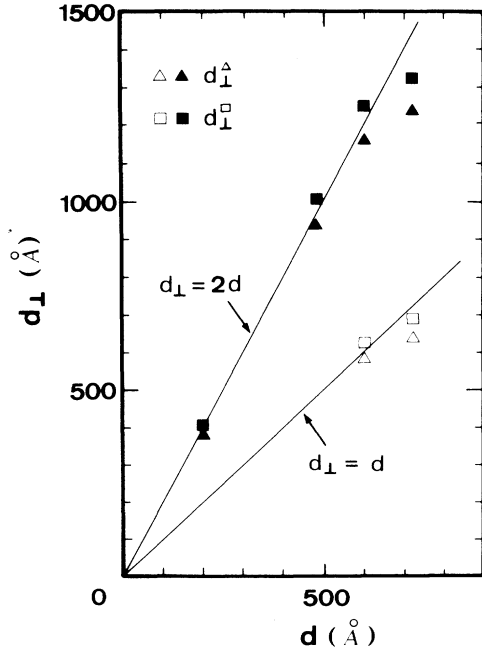


FIG. 16. d_{\perp}^{Δ} , d_{\perp}^{\square} vs multilayer period. Open marks give the values at t_A , and solid ones are at t_B . Solid lines correspond to the singly and double commensurate configurations. Deviations from the commensurate lines for $\lambda = 720 \text{ \AA}$ are probably due to less repetition of deposition (seven times).

tex lattice matches well with the superlattice structure at t_A , and forms a doubly commensurate configuration at t_B .

We would like to note here that dimensional crossover is deeply involved in the singly commensurate configuration mentioned above. Generally speaking, in the three-dimensional region, the lattice spacing of vortices at H_{c2} is expected to decrease continuously as the temperature decreases. The same situation is of course expected for the lattice of superconducting nucleations. We saw that at t_A the vortex lattice falls into the singly commensurate configuration against the multilayer period d . In this case, all nucleations are eventually situated at the superconducting layers. If the superconducting layer is in itself two dimensional, it is hard to think that the lattice spacing of nucleations decreases further even at temperatures below t_A . Thus nucleations keep to stay in the S layers; in other words, the system really trends toward two dimensional.

To address the origin of the observed commensurability effect, we give a brief qualitative discussion. When ξ_{\perp} is larger than the period of proximity-coupled multilayers, a superconducting nucleation spreads over several layers including both superconducting and normal regions. When ξ_{\perp} becomes comparable to the period, the extent of each nucleation reduces and tends preferentially to stay in the S layers. However, this tendency should not always be acceptable, because we can expect that vortices (nucleations) are disposed to form a temperature-dependent regular lattice, as in a homogeneous superconductor. Thus, in superconducting multilayers, vortices (nucleations) probably result in the formation of a complicated lattice, and this effect arising from the commensurability should well be reflected on $H_{c2\parallel}$, although at the present stage we cannot give theoretical corroboration of how this effect causes the upturn in $H_{c2\parallel}$.

A commensurability effect between the superlattice structure and the vortex lattice has been found in the critical current I_c of composition-modulated films in a magnetic field, i.e., I_c is enhanced when the vortex lattice is commensurate with the periodic structure.³⁴ However, our observations on $H_{c2\parallel}$ should be physically distinguished from the effect observed in I_c . The effect seen in I_c results from the collective pinning of the vortex lattice under a field less than $H_{c2\parallel}$, and hence the Lorentz force is involved, while such a force is not concerned with the phenomena for $H_{c2\parallel}$.

Note that there exists some theoretical work^{35,36} which predicts inflections in $H_{c2\parallel}$ similar to our observation at t_B . However, the model investigated there is far from our V-Ag system. The model is such that T_c is spatially constant and only impurity concentration is modulated sinusoidally. Therefore these theories seem not to be relevant to our case.

B. $H_{c2\perp}$

Figure 17 shows $H_{c2\perp}$ as a function of the reduced temperature t . Noticeable features are, first, the zero-temperature extrapolation of $H_{c2\perp}$ rises greatly with d , being quite different from the behavior of the three-dimensional multilayers discussed in the preceding sec-

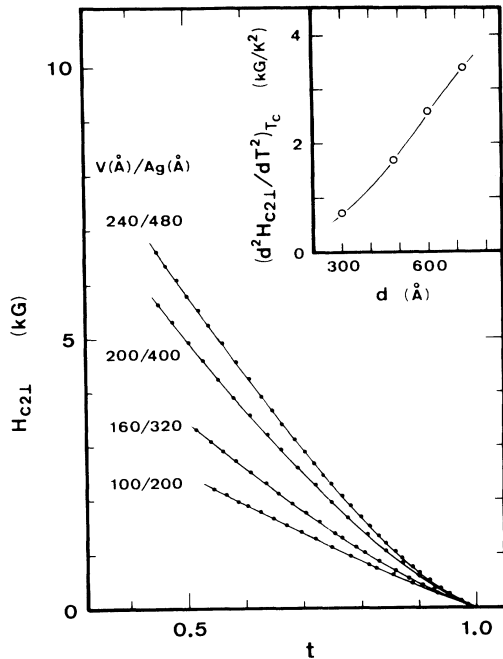


FIG. 17. Upper critical field perpendicular to the layers as a function of the reduced temperature. The thickness ratio of V and Ag is 1:2. Inset shows $(d^2 H_{c2\perp} / dT^2)_{T_c}$ as a function of the multilayer period. Solid curves serve as a guide for the eye.

tion; and second, in contrast with the peculiar variation in $H_{c2\parallel}$, $H_{c2\perp}$ exhibits monotonic upturns, being continuously enhanced with increasing d .

The upturn in $H_{c2\perp}$ has been observed in other multilayers.^{4,37} Haywood and Ast sought its origin, but a definitive conclusion was not reached.³⁷ However, BKC⁹ and TT¹⁰ calculations show that S-N multilayers reveal the upturn in $H_{c2\perp}$ as an intrinsic character involved in the proximity effect.

To characterize the upturn, BKC⁹ calculated the second derivative $(d^2 H_{c2\perp} / dT^2)_{T=T_c}$. According to them, the positive curvature is sensitive to the layer thicknesses (d_S and d_N) as well as to the mean free paths l_S and l_N , i.e., $H_{c2\perp}''(T_c)$ increases with d_S and d_N below several hundred Å, and also increases gradually with l_N as long as l_S is constant.

We evaluated $H_{c2\perp}''(T_c)$ of our samples, which was determined from the slope of $H_{c2\perp} / (T_c - T)$ versus $(T_c - T)$. The result is shown in the inset of Fig. 17 as a function of d , and is in qualitative agreement with the predicted tendency (recall that l_{Ag} is d_{Ag} dependent while l_V is constant for our samples in question).

The TT theory¹⁰ has revealed that the upturn in $H_{c2\perp}$ is enhanced with the increase of the diffusion-constant ratio D_N / D_S (although this part of calculations in their text is performed with such parameters that the S and N layers have the same transition temperature). Moreover, they gave the physical interpretation for the upturn as follows: When a magnetic field is applied perpendicular to the layer, the pair amplitude of nucleation varies periodically

along the vortices. Near T_c , undulation of the amplitude is rather flat. In contrast, when the temperature decreases, the undulation becomes large so that nucleations tend to be confined in the S layers. Consequently, $H_{c2\perp}$ approaches that of the S layers at lower temperature. Since the degree of nucleation confinement in the S layers becomes higher for greater ratio of D_N / D_S , the upturn is expected to be enhanced with the increase of D_N / D_S .

Turning attention to our samples again, D_{Ag} / D_V for the samples treated here is given by $v_{Ag} l_{Ag} / v_V l_V = 0.22 d_{Ag}$, where $l_{Ag} = 1.3 d_{Ag}$ Å and $l_V = 22$ Å (see Sec. II C). Thus we find that D_{Ag} / D_V , which is considered to be partly responsible for the growth of the upturn, varies from 44 for V (100 Å)-Ag(200 Å) up to 106 for V (240 Å)-Ag (480 Å).

Comparing Fig. 17 with Fig. 13, we see that enhancement of the upturn in $H_{c2\perp}$ becomes greater as the degree of two dimensionality in $H_{c2\parallel}$ is higher. Therefore, it seems that the upturn in $H_{c2\perp}$ is more or less correlated to the dimensional crossover in $H_{c2\parallel}$. Considering that both phenomena in $H_{c2\perp}$ and $H_{c2\parallel}$ are concerned with the localization of nucleations in the S layers, one can persuade oneself of the correlation.

VI. CONCLUSIONS

We have investigated the upper critical field ($H_{c2\perp}$ and $H_{c2\parallel}$) of proximity-coupled superconducting multilayers composed of V and Ag. The samples were prepared by ultrahigh-vacuum electron-beam evaporation. From x-ray diffraction analysis, we confirmed that an artificial superlattice structure was successfully attained, where V and Ag have their bulk structures, bcc and fcc, respectively. The stacking structure showed preferential orientation of V(110) and Ag(111) parallel to the film plane.

For the sake of thorough discussion of H_{c2} , the electron mean free path in each layer (l_V and l_{Ag}) was extracted from the normal-state resistivity parallel to the layers: l_V is thickness dependent up to about 100 Å of V-layer thickness, reflecting the V-Ag boundary scattering, and then reaches the intrinsic value of about 22 Å. In contrast, l_{Ag} is restricted almost completely by the boundary scattering and is approximated by 1.3 times of Ag-layer thickness, where the maximum Ag-layer thickness studied is 480 Å.

Referring to the above-derived transport properties, we characterized H_{c2} of three-dimensional multilayers in terms of the parallel coherence length at 0 K, $\xi_{\parallel}(0)$, and the anisotropy of the upper critical field $H_{c2\parallel} / H_{c2\perp}$: $\xi_{\parallel}(0)$ is insensitive to the multilayer period, but depends considerably on the compositional ratio, meaning that the ratio plays a predominant role for determination of $H_{c2\perp}(0)$. The anisotropy is found to be quite small (1.1–1.3), and is rather insensitive to both the multilayer period and the compositional ratio. Our analysis has shown that the above features are well reproduced by the relevant theories, indicating that for the multilayers situated in the three-dimensional regime, a knowledge of the resistivity in each layer provides almost full information on H_{c2} with an aid of these theories.

The temperature dependence of H_{c2} has aroused strong

interest because of its unusual behavior. We have revealed the overall picture of the temperature dependence for our specific system. Experimental observations on $H_{c2\perp}$ are as follows: In the thin-layer limit, $H_{c2\perp}$ varies with temperature in the same manner as homogeneous dirty-limit superconductors. As the layers become thicker, the temperature dependence in the low-temperature region approaches a linear slope, and near T_c , a slight positive curvature appears. This positive curvature is enhanced with a further increase of the multilayer period. Note that systematic enhancement of the positive curvature observed in $H_{c2\perp}$ has been predicted theoretically as an intrinsic nature of the proximity-coupled system.

In contrast with the monotonic variation in $H_{c2\perp}$ with temperature, we found two types of anomalies in the temperature dependence of $H_{c2\parallel}$, i.e., one is a drastic upturn at a certain temperature, and the other is an upward inflection at a higher temperature. Investigation of the coherence length has revealed that these two types of anomalies in $H_{c2\parallel}$ are tightly concerned with the commensurability between the vortex lattice and the multilayer

structure. From the standpoint of dimensionality, the commensurability involved in the former anomaly eventually leads to a crossover from three- to two-dimensions, by which the upturn is greatly enhanced.

It should be noted that the observed correlation between the degree of two dimensionality in $H_{c2\parallel}$ and the enhancement of the positive curvature in $H_{c2\perp}$ can be understood assuming that confinement of nucleation in the S layers is responsible for both features.

ACKNOWLEDGMENTS

Useful discussions with Dr. S. Takahashi, Professor M. Tachiki, Professor T. H. Geballe, and Professor H. Yasuoka are acknowledged. Special thanks are also due to T. Yamada for his cooperation in the sample preparation. The authors wish to express their thanks to Professor Emeritus T. Takada for his continuous interest. This work was supported in part by a grant-in-aid for scientific research from the Ministry of Education, Science, and Culture of Japan.

¹For a review, see S. T. Ruggiero and M. R. Beasley, in *Synthetic Modulated Structures*, edited by L. Chang and B. C. Giessen (Academic, New York, 1985), p. 365.

²See, for example, K. Kanoda, H. Mazaki, T. Yamada, N. Hosoito, and T. Shinjo, *Phys. Rev. B* **35**, 415 (1987).

³R. A. Klemm, A. Luther, and M. R. Beasley, *Phys. Rev. B* **12**, 877 (1975).

⁴S. T. Ruggiero, T. W. Barbee, Jr., and M. R. Beasley, *Phys. Rev. Lett.* **45**, 1299 (1980); *Phys. Rev. B* **26**, 4894 (1982).

⁵I. Banerjee, Q. S. Yang, C. M. Falco, and I. K. Schuller, *Phys. Rev. B* **28**, 5037 (1983).

⁶C. S. L. Chun, G. G. Zheng, J. L. Vicent, and I. K. Schuller, *Phys. Rev. B* **29**, 4915 (1984).

⁷L. Dobrosavljević, *Phys. Status Solidi B* **55**, 773 (1973).

⁸P. G. de Gennes and E. Guyon, *Phys. Lett.* **3**, 168 (1963); N. R. Werthamer, *Phys. Rev.* **132**, 2440 (1963).

⁹K. R. Biagi, V. G. Kogan, and J. R. Clem, *Phys. Rev. B* **32**, 7165 (1985).

¹⁰S. Takahashi and M. Tachiki, *Phys. Rev. B* **33**, 4620 (1986).

¹¹K. Kanoda, H. Mazaki, T. Yamada, N. Hosoito, and T. Shinjo, *Phys. Rev. B* **33**, 2052 (1986).

¹²I. K. Schuller, *Phys. Rev. Lett.* **44**, 1597 (1980).

¹³Y. Endoh, K. Kawaguchi, N. Hosoito, T. Shinjo, T. Takada, Y. Fujii, and T. Ohnishi, *J. Phys. Soc. Jpn.* **53**, 3481 (1984).

¹⁴Y. Fujii, T. Ohnishi, T. Ishihara, Y. Yamada, K. Kawaguchi, N. Nakayama, and T. Shinjo, *J. Phys. Soc. Jpn.* **55**, 251 (1986).

¹⁵M. B. Brodsky, *J. Magn. Magn. Mater.* **35**, 99 (1983).

¹⁶For multilayers with d_{Ag} less than 100 Å, the contribution of the outermost 100-Å Ag layers to the resistivity was subtracted from the raw data.

¹⁷C. M. Soukoulis and D. A. Papaconstantopoulos, *Phys. Rev. B* **26**, 3673 (1982).

¹⁸N. W. Ashcroft and N. D. Mermin, *Solid State Physics* (Holt, Rinehart, and Winston, New York, 1976), pp. 5, 757.

¹⁹G. Deutscher and P. G. de Gennes, in *Superconductivity*, edited by R. D. Parks (Dekker, New York, 1969), Vol. II, p. 1005.

²⁰T. Ishida and H. Mazaki, *Phys. Rev. B* **20**, 131 (1979).

²¹T. H. Geballe, in *Advances in Superconductivity*, edited by B. Deaver and J. Ruvalds (Plenum, New York, 1983), p. 387; R. A. Hein, *Phys. Rev. B* **33**, 7539 (1986).

²²*Quantum Fluids, Proceedings of the Sussex University Symposium*, edited by D. F. Brewer (North-Holland, Amsterdam, 1966), p. 26.

²³J. P. Hurault, *Phys. Lett.* **20**, 587 (1966).

²⁴E. Helfand and N. R. Werthamer, *Phys. Rev. Lett.* **13**, 686 (1964); *Phys. Rev.* **147**, 288 (1966).

²⁵See, for example, the Appendix of T. P. Orlando, E. J. McNiff, Jr., S. Foner, and M. R. Beasley, *Phys. Rev. B* **19**, 4545 (1979).

²⁶K. Maki, *Phys.* **1**, 21 (1964); P. G. de Gennes, *Phys. Kondens. Mater.* **3**, 79 (1964).

²⁷P. G. de Gennes, *Rev. Mod. Phys.* **36**, 225 (1964).

²⁸R. Radebaugh and P. H. Keesom, *Phys. Rev.* **149**, 209 (1966).

²⁹C. Kittel, *Introduction to Solid State Physics* (Wiley, New York, 1976), pp. 154, 167.

³⁰L. R. Testardi and L. F. Mattheiss, *Phys. Rev. Lett.* **41**, 1612 (1978).

³¹W. E. Lawrence and S. Doniach, in *Proceedings of the 12th International Conference on Low Temperature Physics, Kyoto, 1970*, edited by E. Kanda (Academic, Kyoto, 1971) p. 361.

³²G. Deutscher and O. Entin-Wohlman, *Phys. Rev. B* **17**, 1249 (1978).

³³ d_{\perp}^{Δ} is not the nearest-neighbor distance of vortices. Note that in the isotropic case, the latter is given as $(\frac{4}{3})^{1/4} (\phi_0/H_{c2})^{1/2}$ [see M. Tinkham, *Introduction to Superconductivity* (McGraw-Hill, New York, 1975), p. 141], while the former is expressed as $(\frac{3}{4})^{1/4} (\phi_0/H_{c2})^{1/2}$.

³⁴H. Raffy, J. C. Renard, and E. Guyon, *Solid State Commun.* **11**, 1679 (1972); H. Raffy, E. Guyon, and J. C. Renard, *ibid.* **14**, 427 (1974); *ibid.* **14**, 431 (1974).

³⁵S. Ami and K. Maki, *Prog. Theor. Phys.* **53**, 1 (1975).

³⁶L. Dobrosavljević and M. Kulić, *J. Low Temp. Phys.* **32**, 505 (1978).

³⁷T. W. Haywood and D. G. Ast, *Phys. Rev. B* **18**, 2225 (1978).